



HAL
open science

Using simultaneous voltage and calcium imaging to study fast Ca²⁺ channels

Nadia Jaafari, Elodie Marret, Marco Canepari

► **To cite this version:**

Nadia Jaafari, Elodie Marret, Marco Canepari. Using simultaneous voltage and calcium imaging to study fast Ca²⁺ channels. *Neurophotonics*, 2015, 2 (2), pp.021010. 10.1117/1.NPh.2.2.021010 . hal-01324485

HAL Id: hal-01324485

<https://hal.science/hal-01324485>

Submitted on 1 Jun 2016

HAL is a multi-disciplinary open access archive for the deposit and dissemination of scientific research documents, whether they are published or not. The documents may come from teaching and research institutions in France or abroad, or from public or private research centers.

L'archive ouverte pluridisciplinaire **HAL**, est destinée au dépôt et à la diffusion de documents scientifiques de niveau recherche, publiés ou non, émanant des établissements d'enseignement et de recherche français ou étrangers, des laboratoires publics ou privés.

Using simultaneous voltage and calcium imaging to study fast Ca²⁺ channels

Nadia Jaafari^{1,2,3}, Elodie Marret^{1,2,3} and Marco Canepari^{1,2,3}

¹ Inserm U836, Grenoble Institute of Neuroscience, Team 3, Grenoble Cedex 09, France

² Université Joseph Fourier, Laboratoire Interdisciplinaire de Physique (CNRS UMR 5588), France

³ Laboratories of Excellence, Ion Channel Science and Therapeutics

***Address all correspondence to:** Marco Canepari, Laboratoire Interdisciplinaire de Physique (CNRS UMR 5588), Bat. E45, 140 avenue de la physique, Domaine univ., 38402 St Martin d'Hères cedex, France. Email: marco.canepari@ujf-grenoble.fr

Keywords

Calcium imaging, voltage imaging, calcium currents

Abstract

The combination of fluorescence measurements of membrane potential and intracellular Ca^{2+} concentration allows correlating, with spatial precision, the electrical and calcium activity of a cell. The technical advances allowing this type of measurement was achieved only recently and represents an important step in the progress of the voltage imaging approach pioneered, over forty years ago, by Lawrence B Cohen. Here, we show how this approach can be used to investigate the function of Ca^{2+} channels using the foreseen possibility to extract Ca^{2+} currents from imaging experiments. The kinetics of the Ca^{2+} current, mediated by voltage-gated Ca^{2+} channels, can be accurately derived from the Ca^{2+} fluorescence measurement using Ca^{2+} indicators with $K_D > 10 \mu\text{M}$ that equilibrate in less than 1 ms. In this respect, the imaging apparatus dedicated to this application is described in detail. Next, we illustrate the mathematical procedure to extract the current from the Ca^{2+} fluorescence change including a method to calibrate the signal to charge flux density. Finally, we show an example of simultaneous membrane potential and Ca^{2+} optical measurement associated with an action potential at a CA1 hippocampal pyramidal neuron from a mouse brain slice. The advantages and limitations of this novel approach are discussed.

1 Introduction

Since the introduction of organic voltage sensitive dyes¹, the membrane potential (V_m) change associated with neuronal activity could be measured, at multiple cellular sites, using fluorescence.^{2,3} This information, spatially and temporally correlated with Ca^{2+} signals, opens the gate to the understanding of many physiological processes underlying neuronal function.⁴ More recently, voltage sensitive dyes imaging was combined, in single neurons, to Ca^{2+} fluorescence imaging, initially using sequential recordings^{5,6} and later using simultaneous recordings with two aligned cameras⁷. Under general conditions, this experimental strategy allows correlating the change of intracellular Ca^{2+} concentration with the underlying V_m . Nevertheless, if the change of intracellular Ca^{2+} concentration is due exclusively to Ca^{2+} influx through the plasma membrane, the measurement of Ca^{2+} concentration can be in principle converted into a measurement of Ca^{2+} current.⁸ Only in this case, when no Ca^{2+} release from internal stores occurs, the combined optical measurement of V_m using voltage sensitive dyes permits the study of the voltage regulation of Ca^{2+} channels.

The theory of obtaining an optical measurement of a fast Ca^{2+} current starts with the analysis of the dye- Ca^{2+} binding reaction occurring in the presence of an endogenous cellular Ca^{2+} buffer. This scenario has been initially studied by Kao and Tsien⁹ who established that the relaxation time of the dye- Ca^{2+} binding reaction (τ_R) can be approximated by the equation:

$$\tau_R = \frac{1}{K_{ON}^{Dye} \cdot [Ca^{2+}] + K_{OFF}^{Dye}}$$

For all Ca^{2+} indicators, the association constant (K_{ON}^{Dye}) is fast and limited by diffusion, typically to $\sim 6 \cdot 10^8 \text{ M}^{-1} \text{ s}^{-1}$, while the dissociation constant K_{OFF}^{Dye} may vary two order of magnitudes. Thus, τ_R at different free Ca^{2+} concentrations ($[Ca^{2+}]$) can be estimated as a function of the equilibrium constant $K_D^{Dye} = K_{OFF}^{Dye} / K_{ON}^{Dye}$. Whereas for high-affinity indicators with $K_D < 1 \text{ } \mu\text{M}$ τ_R is typically $> 1 \text{ ms}$ and depends on $[Ca^{2+}]$, for low-affinity indicators with $K_D > 10 \text{ } \mu\text{M}$ τ_R is faster (typically $< 200 \text{ } \mu\text{s}$) and does not depend on $[Ca^{2+}]$. This theoretical consideration suggests that a fast Ca^{2+} current with duration of a few milliseconds can be reliably tracked by low-affinity indicators.

While the relaxation time of the dye- Ca^{2+} binding reaction sets the limit of detection of a Ca^{2+} influx, the measurement of a Ca^{2+} current is possible only if the total Ca^{2+} entering the cell through the plasma membrane is proportional to the Ca^{2+} bound to the dye. In a previous report, we described the conditions under which this requirement is fulfilled.¹⁰ In addition, we demonstrated that this is the case of the Ca^{2+} signal associated with the action potential in the CA1 pyramidal neuron of the hippocampus.¹⁰

Here, we describe more in detail how to achieve these measurements. In particular, we describe the necessary apparatus as well as the methodological aspects of this novel approach. We report tests

with five Ca²⁺ indicators (Oregon Green 488 BAPTA-1, Oregon Green 488 BAPTA-6F, Oregon Green 488 BAPTA-5N, Bis-Fura2, and FuraFF) and, for the low-affinity indicators, confirmed their ability to track a Ca²⁺ current by performing computer simulations. We also describe an alternative approach of data analysis using the fit of the Ca²⁺ transient to obtain the Ca²⁺ current from a reduced number of trials. We finally further discuss how this novel approach overcomes the limitations of Ca²⁺ current measurements using electrode techniques.

2 Materials and Methods

2.1 Slice preparation, solutions and electrophysiology

Experiments were approved by the Isere prefecture (Authorisation n. 38 12 01) and the specific protocol (n.197) by the ethics committee of the Grenoble Institute of Neuroscience. Hippocampal slices (250 µm thick) were prepared from 21-35 postnatal days old C57Bl6 mice as previously described¹¹ using either a VF-200 compressstome (Precisionary Instruments, Greenville, NC) or a Leica VT1200 (Leica, Wetzlar, Germany). Slices were cut in iced extracellular solution and incubated at 37°C for 1 hr before use. The extracellular solution used contained (in mM): 125 NaCl, 26 NaHCO₃, 1 MgSO₄, 3 KCl, 1 NaH₂PO₄, 2 CaCl₂ and 20 glucose, bubbled with 95% O₂ and 5% CO₂. The intracellular solution contained (in mM): 125 KMeSO₄, 5 KCl, 8 MgSO₄, 5 Na₂-ATP, 0.3 Tris-GTP, 12 Tris-Phosphocreatine, 20 HEPES, adjusted to pH 7.35 with KOH. To block Na⁺ and K⁺ channels in voltage clamp experiments, the external solution also contained 1 µM tetrodotoxin, 5 mM tetraethylammonium (TEA), 4 mM 4-aminopyridine and 250 nM apamin, and the internal solution also contained 5 mM TEA. In this work, five Ca²⁺ indicators (all purchased from Invitrogen, Carlsbad, CA) were used at the concentration of 1 mM: Oregon Green 488 BAPTA-1 (OGB1, K_D = 0.21 µM¹²), Oregon Green 488 BAPTA-6F (OG6F, K_D = 3 µM, as reported by the vendor), Oregon Green 488 BAPTA-5N (OG5N, K_D = 35 µM¹³), Bis-Fura2 (BF2, K_D = 0.53 µM, as reported by the vendor) and FuraFF (K_D = 10 µM¹⁴). Ca²⁺ indicators were dissolved directly into the internal solution. In voltage-imaging experiments, cells were loaded as previously described⁴ with the voltage-sensitive dye JPW1114 (Invitrogen). In calibrating experiments using the Ca²⁺-releasing caged compound nitrophenyl-EGTA (NP-EGTA)¹⁵ (Invitrogen), the internal solution also contained 150 µM CaCl₂. All other chemicals were purchased either from Tocris (Bristol, UK) or Sigma-Aldrich (St. Louis, MO). Experiments were performed at 32-34 °C using an Olympus BX51 microscope equipped with a 60X/1.0 NA Nikon objective. Patch-clamp recordings were made using a Multiclamp amplifier 700A (Molecular Devices, Sunnyvale, CA) and voltage and current signals

were acquired with the A/D board of the CCD camera. The V_m measured with the patch pipette was corrected for the junction potential (-11 mV) as calculated with the JPCalc software.¹⁶ In voltage clamp recordings, the Ca^{2+} current was evoked by depolarising pulses from -70 mV to -10 mV and measured in the soma by subtracting the scaled subthreshold current associated with a voltage step from -70 mV to -60 mV.

2.2 The imaging system

A schematic of the imaging system is shown in Fig. (1a). Simultaneous UV/blue LED illumination from the epifluorescence port of the microscope was allowed by a 409 nm dichroic mirror (FF409, Semrock, Rochester, New York). UV light was either at 365 nm for photolysis or at 385 nm for excitation of Fura indicators fluorescence. The 365 nm LED was controlled by an OptoFlash (CAIRN Research Ltd., Faversham, UK) and the other LEDs controlled by an OptoLED (Cairn). The image could be demagnified either by 0.5 or by 0.25 obtaining the fields of view shown in Fig. (1b). The two image were separated by a 593 nm dichroic mirror and acquired with a dual-head NeuroCCD-SMQ camera (Redshirt, Decatur, GA) at 510 ± 42 nm (with the “ Ca^{2+} CCD”) and at >610 nm (with the “ V_m CCD”). The Ca^{2+} image was therefore the mirrored picture of the V_m image. Whereas the camera has 80X80 pixels per head (full resolution), to achieve the speed of 20 kHz, binned stripes of 26×4 pixels were imaged. To achieve simultaneous illumination and detection of OG5N and JPW1114, both indicators were excited at 470 nm. The sensitivity of the VSD at 470 nm was about 4 times less than that at 532 nm. Thus, while an action potential is associated with a fractional change of fluorescence ($\Delta F/F_0$) of 2-8% in the proximal apical dendrite at 532 nm, the same signal is associated with $\Delta F/F_0$ of 0.5-2% at 470 nm. Using this configuration, the emission of JPW1114 detected by the Ca^{2+} CCD is negligible as shown in Fig. (1c) and the emission of OG5N detected by the V_m CCD is also negligible as shown in Fig. (1d). Thus, it is possible to discriminate and quantify Ca^{2+} fluorescence from V_m fluorescence.

2.3 Recording and analysis of Ca^{2+} and V_m optical signals

Ca^{2+} and V_m recordings, were performed at 20 kHz and data were initially expressed as $\Delta F/F_0$. The high acquisition rate was necessary to prevent the loss of temporal information while applying the filtering procedure described below. Ca^{2+} recordings started 20-25 minutes after establishing the whole cell configuration, i.e. the time necessary to achieve the equilibrium of the indicator over the dendritic segment of recording. To improve the signal-to-noise ratio (S/N), fluorescence was generally averaged over 9-64 trials as specified in each figure legend and corrected for bleaching

using trials without signal. All data analysis was performed using software written in Matlab (The Mathworks, Natick, MA). The JPW1114- $\Delta F/F_0$ signal was calibrated in terms of V_m change using a previously demonstrated protocol based on wide-field photorelease of L-glutamate from the caged compound 4-methoxy-7-nitroindoliny-caged-L-glutamate (MNI-glutamate).¹⁷ Briefly, a calibration of the JPW1114- $\Delta F/F_0$ signal can be done if an electrical signal of known amplitude is available at all recordings sites. In many neuronal types, activation of a large portion of ionotropic glutamate receptors makes them the dominant conductance and the resulting V_m will be 0 mV in all the illuminated area. In CA1 hippocampal pyramidal neurons a calibration is possible since the resting V_m is uniform over the whole cell.¹⁸ Thus, the JPW1114- $\Delta F/F_0$ signal associated with a saturating photorelease of L-glutamate will correspond to a change of V_m from the resting V_m to 0 mV. A representative cell where this procedure was applied is shown in Fig. (2a). The JPW1114- $\Delta F/F_0$ signal associated with an action potential was recorded from the initial 50 μm apical dendritic segment of a CA1 hippocampal pyramidal neuron (Fig. 2b). After this recording, we added 1 μM TTX to block voltage-gated Na^+ channels and 1 mM MNI-glutamate to the external solution. Starting from the resting V_m (-60 mV), we uncaged L-glutamate producing a depolarisation to 0 mV. The glutamate-induced optical signal (Fig. 2b, green) provided the calibration for the action potential. Statistical significance was evaluated using either the paired t-test or the two-population (2P) t-test.

2.4 Computer simulations

The results of the analysis of the kinetics of the five Ca^{2+} indicators were compared with those obtained by computer simulations using a previously published theoretical framework.¹⁹ Briefly, we simulated the reaction of the dye ([D]) with Ca^{2+} in the presence of 1 mM of an endogenous buffer ([B]). For comparison with voltage clamp experiments, using as Ca^{2+} current (I_{Ca}) the current measured with the patch electrode, we numerically solved the set of differential equations:

$$\frac{d[\text{Ca}^{2+}]}{dt} = I_{\text{Ca}} - K_{\text{ON}}^{\text{D}} \cdot [\text{Ca}^{2+}] \cdot [\text{D}] + K_{\text{OFF}}^{\text{D}} \cdot [\text{DCa}^{2+}] - K_{\text{ON}}^{\text{B}} \cdot [\text{Ca}^{2+}] \cdot [\text{B}] + K_{\text{OFF}}^{\text{B}} \cdot [\text{BCa}^{2+}]$$

$$\frac{d[\text{DCa}^{2+}]}{dt} = K_{\text{ON}}^{\text{D}} \cdot [\text{Ca}^{2+}] \cdot [\text{D}] - K_{\text{OFF}}^{\text{D}} \cdot [\text{DCa}^{2+}]$$

$$\frac{d[\text{BCa}^{2+}]}{dt} = K_{\text{ON}}^{\text{B}} \cdot [\text{Ca}^{2+}] \cdot [\text{B}] - K_{\text{OFF}}^{\text{B}} \cdot [\text{BCa}^{2+}]$$

$$\frac{d[\text{D}]}{dt} = - \frac{d[\text{DCa}^{2+}]}{dt}$$

$$\frac{d[\text{B}]}{dt} = - \frac{d[\text{BCa}^{2+}]}{dt}$$

The value of the association and equilibrium constants of the endogenous buffer were $K_{\text{ON}}^{\text{B}} = 2 \cdot 10^8 \text{ M}^{-1} \text{ s}^{-1}$ and $K_{\text{D}}^{\text{B}} = 10^{-5} \text{ M}$ while $K_{\text{OFF}}^{\text{B}} = K_{\text{ON}}^{\text{B}} \cdot K_{\text{D}}^{\text{B}}$. The value of the association constant of all Ca^{2+}

indicators was $K_{ON}^D = 6 \cdot 10^8 \text{ M}^{-1} \text{ s}^{-1}$, as reported by Kao and Tsien⁹ while $K_{OFF}^D = K_{ON}^D \cdot K_D^D$ was derived for each different indicator from the K_D values reported above. Numerical solutions were obtained using the Matlab function “ode45”.

3 Results

3.1 Comparative analysis of the kinetics of different Ca^{2+} indicators.

The theoretical considerations described in the Introduction suggest that the kinetics of a fast Ca^{2+} current with duration of a few milliseconds can be reconstructed from the fluorescence change of a low-affinity indicator. The ultimate strategy to test this hypothesis is to verify that the $\Delta F/F_0$ Ca^{2+} signal is linear with the integral of the Ca^{2+} current measured, under voltage clamp, in the presence of Na^+ and K^+ blockers (see Materials and Methods). The protocol used in these tests, illustrated in Fig. (3a), consisted in two depolarising square pulses. The current associated with the first pulse, from -70 mV to -60 mV not evoking a Ca^{2+} current, was scaled and subtracted from the current associated with a pulse from -70 mV to +10 mV. This procedure permitted the extraction of the Ca^{2+} current from the total current recording containing the leak current and the capacity transient. The integral of the Ca^{2+} current obtained in this way was then compared to the $\Delta F/F_0$ signal. Fig. (3b) shows results from five representative cells each recorded with a different indicator: the first 7 ms of I_{Ca} normalised to 1 (black traces), the corresponding normalised I_{Ca} integrals (red traces) and the associated normalised $\Delta F/F_0$ signals (blue traces). The signals obtained in these experiments were faithfully mimicked by the results of computer simulations, reported on the right, performed as described in the Materials and Methods.

To quantify the difference of kinetics between the Ca^{2+} $\Delta F/F_0$ signal and the I_{Ca} integral we computed the area (“S”) of the difference of the two curves normalised to 1 over the first 4 ms as shown in Fig. (3c). The statistics of S for the five groups of cells (N = 4-12 for each indicator) is illustrated in Fig. (3d). The values of S with the two low-affinity indicators OG5N and FuraFF, were statistically different from the values of S with the high-affinity indicators OGB1 and BF2 (2P T-test, $p < 0.02$). In particular, the low affinity indicators were able of tracking fast Ca^{2+} currents. OG5N- $\Delta F/F_0$ has S/N more than times 3 larger than FuraFF- $\Delta F/F_0$ associated with the same Ca^{2+} signal. For this reason OG5N should be used for measuring relative small Ca^{2+} currents as those reported here. However, FuraFF can be better combined with JPW1114 for simultaneous V_m and Ca^{2+} imaging⁷ and should be used for larger Ca^{2+} currents where fluorescence averaging over many trials is less critical.

The tests presented here suggest that all organic Ca^{2+} indicators with K_D for Ca^{2+} of more than $10 \mu\text{M}$ can be potentially used to faithfully extract the time-course of a fast Ca^{2+} current.

3.2 Calibration of the OG5N- $\Delta F/F_0$ signal and extraction of the Ca^{2+} current

An important aspect of the Ca^{2+} imaging technique is its ability to provide an estimate of the intracellular Ca^{2+} concentration. In general terms, this estimate is not straightforward since the important information may involve knowing the free Ca^{2+} concentration ($[\text{Ca}^{2+}]_{\text{FREE}}$) as well as the Ca^{2+} that binds to the dye and to the endogenous buffer. However, for a quantitative estimate of I_{Ca} , the important information is exclusively the total Ca^{2+} concentration ($[\text{Ca}^{2+}]_{\text{TOT}}$) entering the cell. The estimate of $[\text{Ca}^{2+}]_{\text{TOT}}$ corresponding to a particular $\Delta F/F_0$ signal will allow determining the charge concentration and deriving the corresponding I_{Ca} volume density (I_{Ca}/V).

A way to produce a $[\text{Ca}^{2+}]_{\text{TOT}}$ of known amplitude is to release Ca^{2+} from a caged compound. The cell in Fig. (4a) was filled with an intracellular solution also containing $300 \mu\text{M}$ of NP-EGTA and $150 \mu\text{M}$ CaCl_2 . NP-EGTA before photolysis is a high-affinity Ca^{2+} chelator ($K_D = 80 \text{ nM}$). The K_D decreases by a factor of 12,500 after photolysis.¹⁵ While in the pipette 50% of the NP-EGTA is bound to Ca^{2+} , this percentage is unknown in the cell where it is regulated by the global Ca^{2+} homeostasis. However, when the cell of Fig. (4a) was depolarised from -70 to -10 mV , a persistent OG5N- $\Delta F/F_0$ signal $>20\%$ was observed. Since this signal typically corresponds to >10 times the signal associated with one action potential and $[\text{Ca}^{2+}]_{\text{FREE}}$ associated with an action potential in this dendrite type is $>100 \text{ nM}$ ²⁰, $[\text{Ca}^{2+}]_{\text{FREE}}$ at -10 mV is $>1 \mu\text{M}$. Since K_D of NP-EGTA is 80 nM , at $V_m = -10 \text{ mV}$, more than 92% of NP-EGTA is always bound to Ca^{2+} . Under this condition, as shown in Fig. (4a), the Ca^{2+} indicator is still not saturated since a further depolarization step of $+50 \text{ mV}$ produced a OG5N- $\Delta F/F_0$ signal $>20\%$. Having established that at $V_m = -10 \text{ mV}$, $\sim 300 \mu\text{M}$ is bound to NP-EGTA and available for release, the calibration protocol illustrated in Fig. (4b) consisted in applying a sequence of 16 UV pulses (of 20 ms duration every 5 s) and by measuring the OG5N- $\Delta F/F_0$ signal associated with each pulse. The $[\text{Ca}^{2+}]_{\text{TOT}}$ released at the pulse k follows the geometric progression.²¹

$$[\text{Ca}^{2+}]_{\text{TOT}}(k) = \alpha \cdot (300 \mu\text{M} - \sum_{j=0}^{k-1} [\text{Ca}^{2+}]_{\text{TOT}}(j))$$

where $[\text{Ca}^{2+}]_{\text{TOT}}(k=0) = 0$. The OG5N- $\Delta F/F_0$ corresponding to a given $[\text{Ca}^{2+}]_{\text{TOT}}$ is obtained by fitting this geometric progression to the sequential decrease of the OG5N- $\Delta F/F_0$ amplitude. In this particular cell, we obtained that a OG5N- $\Delta F/F_0$ of 1% corresponded to $[\text{Ca}^{2+}]_{\text{TOT}} = 18 \mu\text{M}$. From this calibration the I_{Ca}/V associated with the action potential was derived in the following way, as shown in Fig. (4c). First, the $\Delta F/F_0$ signal was converted into a charge-to-volume ratio (Q/V) using the

equation:

$$Q/V = \frac{[Ca^{2+}]_{TOT} \cdot 2e \cdot N_A}{dm^3}$$

where e is the fundamental charge, dm is the decimetre unit and N_A is the Avogadro number. Second, the converted signal was filtered using a Savitzky-Golay filter preserving the kinetics of the original signal.²² Finally, the I_{Ca}/V was obtained by applying the time derivative to the filtered signal as shown in Fig. (4c). Previously reported data analysis using this calibration procedure indicated that the $[Ca^{2+}]_{TOT}$ corresponding to a OG5N- $\Delta F/F_0$ signal of 1% varies from 16 μM to 24 μM .¹⁰ Thus, a standard estimate of OG5N- $\Delta F/F_0 = 1\%$ corresponding to $[Ca^{2+}]_{TOT} = 20 \mu M$ can be applied in cells where the calibration protocol is not directly performed.

3.3 Estimate of I_{Ca}/V signals by $\Delta F/F_0$ filtering or curve fitting

The OG5N- $\Delta F/F_0$ signal associated with an action potential can be measured from a 50 μm dendritic segment with good S/N which can be further improved by averaging several trials. The extraction of I_{Ca}/V , however, is based on the calculation of the time derivative which requires the signal noise to be smaller than the signal change between two consecutive samples. A way to obtain this condition is to temporally filter the signal up to the limit of distortion of its kinetics. In our previous report we have shown that the Savitzky-Golay algorithm is an optimal filtering tool permitting for improving the S/N of the OG5N- $\Delta F/F_0$ signal without significant temporal distortion using time-windows of up to 20-30 samples.¹⁰ The application of this procedure allows extracting I_{Ca}/V from relatively large dendritic compartments and by averaging several trials. The challenge for the improvement of data analysis was to go beyond the limitations of the filtering approach. This can be done by fitting the raw or the filtered OG5N- $\Delta F/F_0$ signal with a model function obtaining a noiseless curve that mimics the time course of the OG5N- $\Delta F/F_0$ signal. While the choice of the model might be arbitrary, a simple function that resembles the time course of the OG5N- $\Delta F/F_0$ transient is the sigmoid. In particular, the OG5N- $\Delta F/F_0$ signal normalised to its asymptotic value can be mimicked by the products of N sigmoid functions Y

$$Y(t) = \prod_{j=1}^{N_{Sigm}} \frac{1}{1 + e^{-\phi_j \cdot (t - \theta_j)}}$$

where t is time, ϕ_j and θ_j are the parameters to be determined by the fit and N_{Sigm} is the arbitrary number of sigmoid functions. We tried several integer values for N_{Sigm} and we found that 3 was the minimum number of sigmoid functions always providing a fit with the same kinetics of the OG5N- $\Delta F/F_0$ signal. The product of three sigmoid functions was therefore set as the general model to fit the signal and its ability to extract I_{Ca}/V either from small dendritic regions or from relatively large

regions in single trials was assessed in the cell reported in Fig. (5a). In particular, we analyzed signals associated with an action potential from an average of 32 trials or from a single trial (Fig. (5b)). Fig. (5c) shows the $\Delta F/F_0$ signals from the average of 32 trials in a large dendritic region of $\sim 50 \mu\text{m}$ length (region A) and in a small dendritic site of $\sim 2.4 \mu\text{m}$ (region B). The same panel (right traces) also shows the $\Delta F/F_0$ signal in region A from the single trial. Each raw signal was filtered with the Savitzky-Golay algorithm at a time-window of 10, 20 or 40 samples. Alternatively it was fitted with the three-sigmoid model. The filtering algorithm improves the S/N but starts producing a temporal distortion at 40 samples. The consequent distortion of the extracted I_{Ca}/V is evident in the case of the average of 32 trials in region A shown in the left column of Fig. (5d). While in this case the I_{Ca}/V obtained by filtering with a time window of 20 samples has acceptable S/N, the same filtering approach applied to extract I_{Ca}/V either from region B or from region A in a single trail generates a noisy signal (middle and right traces). In all cases, however, the fit approach generates noiseless curves that faithfully reproduce the time-course of the OG5N- $\Delta F/F_0$ signals from which I_{Ca}/V signals can be extracted. This technical improvement in data analysis is critical for many applications. In particular, when spikes occurrence is stochastic, I_{Ca}/V must be extracted from single trials. Alternatively, the gain in analysis performance can be spent to extract I_{Ca}/V from small or relatively dim regions.

3.4 Simultaneous V_m and I_{Ca}/V optical measurements

To illustrate the ability of simultaneous V_m and I_{Ca}/V optical measurements to investigate Ca^{2+} currents and the behaviour of underlying Ca^{2+} channels, we report here an analysis of the I_{Ca}/V associated with an action potential in the initial segment of the apical dendrite of the CA1 hippocampal pyramidal neuron. In the cell of Fig. (6a), action potentials were evoked by current injection and recorded optically in the first $50 \mu\text{m}$ dendritic segment as reported in the top of Fig. (6b). One action potential was evoked starting from $V_m = -60 \text{ mV}$ and another action potential was evoked starting from $V_m = -80 \text{ mV}$. The simultaneously recorded I_{Ca}/V signals are shown in the bottom of Fig. (6b). The I_{Ca}/V associated with the action potential starting from $V_m = -80 \text{ mV}$ was larger than the I_{Ca}/V associated with the action potential starting from $V_m = -60 \text{ mV}$. The time-course of I_{Ca}/V can be precisely correlated with the time-course of V_m as shown in Fig. (6c). In 14 cells in which this protocol was applied, the mean \pm S.E.M. of the I_{Ca}/V peak in the first $50 \mu\text{m}$ dendritic segment was $7.2 \pm 1.7 \text{ pA}/\mu\text{m}^3$ for the action potential starting at $V_m = -60 \text{ mV}$ and $10.1 \pm 1.4 \text{ pA}/\mu\text{m}^3$ for the action potential starting at $V_m = -80 \text{ mV}$ as shown in Fig. (6d). The I_{Ca}/V was consistently larger for the action potential starting at $V_m = -80 \text{ mV}$ ($p < 0.001$, paired t-test). As demonstrated in a previous report¹⁰, the different I_{Ca}/V amplitude observed under the two V_m

conditions was mainly due to activation of T-type voltage-activated Ca^{2+} channels which recovered from inactivation when the cell was hyperpolarised to $V_m = -80$.²⁴

4 Discussion

Since the introduction of organic voltage sensitive dyes and thanks to the work of Lawrence B Cohen and colleagues, it was expected that the improved S/N of V_m measurements²⁴ could open the gate to applications where an imaging approach could eventually overcome the intrinsic limitations of electrode techniques. The more recent introduction of fluorescent V_m probes that could be directly injected into cells²⁵ allowed recordings of V_m of less than 1 mV.²⁶

The patch clamp technique, however, is routinely used to measure not only V_m , but also the membrane current in “voltage clamp” mode. Our current understanding of ion channel function is mainly derived from the use of the patch-clamp techniques. This measurement, in single-electrode or two-electrode voltage clamp, consists in maintaining the cell at a given V_m by compensating the cell current with an injected current.²⁷ The current measured with the electrode is therefore the summation of the filtered currents from all different cellular regions, including remote regions where V_m is unclamped.²⁸ To study the function of native ion channels at different sites of neurons and under physiological electrical activity, this approach is practically not applicable for a series of reasons. First, the “voltage-clamp” condition is not applicable in a cell where V_m is not uniform. Second, although local current measurements from a limited number of cellular sites can be obtained using dendritic patch clamp recordings²⁹, not only the number of recording sites is limited with respect to an imaging approach but each current is also the summation of currents from different sites, filtered with respect to the site of recording. In other words, a voltage-clamp current measurement carries no information on the site of origin of the current. Third, the physiological behaviour of a channel occurs when V_m changes physiologically, which is not the condition of “voltage clamp”. Injecting a current to dynamically clamp the cell and reproducing a physiological V_m change, for instance an action potential, does not solve the problem since the potential drop due to the series resistance and the space-clamp of the cell will generate a non uniform distortion of the V_m form. Fourth, separation of a current mediated by a specific ion requires pharmacological block of all other currents. Obviously, these channels are necessary for a physiological V_m change. For instance, an action potential requires Na^+ , K^+ and Ca^{2+} channels and the study of a specific current during this event would require the block of the other two currents.

For Ca^{2+} currents, the imaging approach described in this report potentially overcomes all these limitations. In contrast to patch-clamp recordings, these calcium optical currents can be measured in conditions of a physiological change of V_m . The measured currents are confined to the sites where they are recorded. The additional information on local V_m change, necessary to correlate the behaviour of the conductance with its biophysical properties, is obtained by performing combined V_m and Ca^{2+} imaging experiments. The possibility to extract I_{Ca} from Ca^{2+} imaging experiments was foreseen in the past. Thus, as expected by the pioneering study of Kao and Tsien⁹ and by the computer simulations reported here, the kinetics of I_{Ca} can be reconstructed without distortion and correlated with V_m change. The crucial information on the V_m at the same site of the I_{Ca} is given by the concomitant V_m optical measurement. In this way, it is possible to follow the activation and deactivation of the channel as a function of the V_m change during physiological activity. The optical measurement of I_{Ca} is however affected by some limitations. First, obviously, it cannot be performed when a concomitant Ca^{2+} release from internal stores occurs. Second, it cannot be applied to measure a slow I_{Ca} that occurs at the same time scale of Ca^{2+} sequestration and extrusion. This, as shown in a previous report¹⁰, will introduce a “negative current” artefact in the I_{Ca} measurement. Third, in the optical measurement, the calibration can be provided in terms of I_{Ca}/V , while the evaluation of I_{Ca} requires precise morphological reconstruction of the site of recording.

The optical measurements of I_{Ca} became possible only recently thanks to the remarkable advance in light sources and detection devices for V_m and ion imaging.³⁰ The simultaneous measurement of V_m and I_{Ca}/V can be also achieved using the low-affinity indicator Fura-FF and the optical settings described in a previous article.⁷ The S/N of Fura-FF $\Delta F/F_0$ signal, however, is substantially lower compared to the equivalent OG5N- $\Delta F/F_0$ signal. Another possibility for simultaneous measurements of V_m and I_{Ca}/V using OG5N is its combination with a red-excitable voltage-sensitive dye such as those described in Yan et al. 2012.^{31,32} Such indicators would allow combining simultaneous blue illumination for OG5N with red optimal illumination for the voltage-sensitive dye. Among these indicators we tested Di-2-ANBDQ(F)PTEA and we found that its fluorescence excited at 470 nm decreases in intensity when V_m is depolarized (data not shown). Thus, when exciting Di-2-ANBDQ(F)PTEA at 470 nm and at 630 nm simultaneously, the $\Delta F/F_0$ signal associated with a V_m change is smaller than the equivalent $\Delta F/F_0$ signal obtained by red illumination only. Finally, for signals that are consistent from trial to trial, measurements of V_m and I_{Ca}/V can be obtained sequentially with the combination of JPW1114 and OG5N by alternating optimal excitation of Ca^{2+} fluorescence at 470 nm with optimal excitation of V_m fluorescence at 532 nm.

The present approach should drastically improve our understanding of the physiological function of Ca^{2+} channels by providing the possibility to explore the biophysics of native channels during physiological activity in subcellular loci of the complex neuronal architecture. The method described

here is, therefore, another important brick in long history of membrane potential imaging applications.

Acknowledgements

We thank Philippe Moreau for technical help and Jean-Claude Vial for useful discussions. This work was supported by the *Agence Nationale de la Recherche* (Grant *Voltimagmicro*, program *Emergence-10*, Labex *Ion Channels Science and Therapeutics*: program number ANR-11-LABX-0015 and National Infrastructure France Life Imaging “Noeud Grenoblois”).

Biographies

Nadia Jaafari obtained her PhD from the University of Marseille and worked, for several years, in the laboratory of J.M. Henley at Medical Research Council Centre for Synaptic Plasticity in Bristol. She is currently INSERM senior research associate in the laboratory of Marco Canepari.

Elodie Marret graduated from the University Joseph Fourier in Grenoble and she is currently INSERM technician in the laboratory of Marco Canepari.

Marco Canepari is INSERM first-class researcher (CR1) working in the “Laboratoire Interdisciplinaire de Physique” in Grenoble. He obtained his PhD at SISSA/ISAS in Trieste and he worked in several laboratories as postdoctoral scientist including the laboratory of Dejan Zecevic at Yale University School of Medicine.

References

1. L. B. Cohen et al., "Changes in axon fluorescence during activity: molecular probes of membrane potential," *J. Membr. Biol.* **19**(1), 1-36 (1974).
2. L. B. Cohen, B. M. Salzberg, and A. Grinvald A, "Optical methods for monitoring neuron activity," *Annu. Rev. Neurosci.* **1**,171-182 (1978).
3. M. Zochowski et al., "Imaging membrane potential with voltage-sensitive dyes," *Biol; Bull.* **198**(1), 1-21 (2000).
4. M. Canepari, K. Vogt, and D. Zecevic, "Combining voltage and calcium imaging from neuronal dendrites," *Cell. Mol. Neurobiol.* **58**(8), 1079-1093 (2008).
5. M. Canepari, M. Djuricic, and D. Zecevic, "Dendritic signals from rat hippocampal CA1 pyramidal neurons during coincident pre- and post-synaptic activity: a combined voltage- and calcium-imaging study," *J. Physiol.* **580**(2), 463-484 (2007).
6. M. Canepari and K. E. Vogt, "Dendritic Spike Saturation of Endogenous Calcium Buffer and Induction of Postsynaptic Cerebellar LTP," *PLoS ONE* **3**(12), e4011 (2008).
7. K. E. Vogt, et al., "High-resolution simultaneous voltage and Ca²⁺ imaging," *J. Physiol.* **589**(3), 489-494 (2011).
8. B.L. Sabatini and W.G. Regehr, "Optical measurement of presynaptic calcium currents," *Biophys. J.* **74**(3), 1549-1563 (1998).
9. J.P.Kao and Tsien R.Y, "Ca²⁺ binding kinetics of fura-2 and azo-1 from temperature-jump relaxation measurements," *Biophys. J.* **53**(4), 635-639 (1988).
10. N. Jaafari, M. De Waard, and M. Canepari, "Imaging Fast Calcium Currents beyond the Limitations of Electrode Techniques," *Biophys. J.* **107**(6), 1280-1288 (2014).
11. N. Jaafari et al., Economic and simple system to combine single-spot photolysis and whole-field fluorescence imaging. *J. Biomed. Opt.* **18**(6), 60505 (2013).
12. B. L. Sabatini, T. G. Oertner, and K. Svoboda, "The life cycle of Ca(2+) ions in dendritic spines," *Neuron* **33**(3), 439-452 (2002).
13. M. Canepari and D. Ogden, "Kinetic, pharmacological and activity-dependent separation of two Ca²⁺ signalling pathways mediated by type 1 metabotropic glutamate receptors in rat Purkinje neurones," *J. Physiol.* **573**(1), 65-82 (2006).
14. R. Schneggenburger and E. Neher, "Intracellular calcium dependence of transmitter release rates at a fast central synapse," *Nature* **406**(6798), 889-893 (2000).
15. G. C. Ellis-Davies and J. H. Kaplan, "Nitrophenyl-EGTA, a photolabile chelator that selectively binds Ca²⁺ with high affinity and releases it rapidly upon photolysis," *Proc. Natl. Acad. Sci. USA* **91**(1), 187-191 (1994).

16. P.H. Barry, "JPCalc, a software package for calculating liquid junction potential corrections in patch-clamp, intracellular, epithelial and bilayer measurements and for correcting junction potential measurements," *J. Neurosci. Meth.* **51**(1), 107-116 (1994).
17. K. E. Vogt, et al., "Combining membrane potential imaging with L-glutamate or GABA photorelease," *PLoS ONE* **6**(10), e24911 (2011).
18. S. Gasparini and J. C. Magee, "Phosphorylation-dependent differences in the activation properties of distal and proximal dendritic Na⁺ channels in rat CA1 hippocampal neurons," *J. Physiol.* **541**(3), 665-672 (2002).
19. M. Canepari and F. Mammano, "Imaging neuronal calcium fluorescence at high spatio-temporal resolution," *J. Neurosci. Methods* **87**(1), 1-11 (1999).
20. M. Maravall et al., "Estimating intracellular calcium concentrations and buffering without wavelength ratioing," *Biophys. J.* **78**(5): 2655-2667 (2000).
21. M. Canepari et al., "Photochemical and pharmacological evaluation of 7-nitroindolyl- and 4-methoxy-7-nitroindolyl-amino acids as novel, fast caged neurotransmitters," *J. Neurosci. Methods* **112**(1): 29-42 (2001).
22. A. Savitzky and M. J. E. Golay, "Smoothing and Differentiation of Data by Simplified Least Squares Procedures," *Analytical Chemistry* **36**, 1627-1639 (1964).
23. C. C. Kuo and S. Yang, "Recovery from inactivation of T-type Ca²⁺ channels in rat thalamic neurons," *J. Neurosci.* **21**(1), 1884-1892 (2001).
24. W. N. Ross et al., "A large change in dye absorption during the action potential," *Biophys. J.* **14**(12), 983-986 (1974).
25. S. Antic and D. Zecevic, "Optical signals from neurons with internally applied voltage-sensitive dyes," *J. Neurosci.* **15**(2), 1392-1405 (1995).
26. M. Canepari et al., "Imaging Inhibitory Synaptic Potentials Using Voltage Sensitive Dyes," *Biophys. J.* **98**(9), 2032-2040 (2010).
27. B. Sakmann and E. Neher, "Patch clamp techniques for studying ionic channels in excitable membranes," *Annu. Rev. Physiol.* **46**, 455-472 (1986).
28. S. R. Williams and S. J. Mitchell, "Direct measurement of somatic voltage clamp errors in central neurons," *Nat. Neurosci.* **11**(7), 790-798 (2008).
29. G. J. Stuart and N. Spruston, "Probing dendritic function with patch pipettes," *Curr. Opin. Neurobiol.*, **5**(3), 389-394 (1995).
30. R. Davies, J. Graham, and M. Canepari, "Light Sources and Cameras for Standard in Vitro Membrane Potential and High-Speed Ion Imaging," *J. Microsc.* **251**(1), 5-13 (2013).
31. W. L. Zhou, P. Yan, J. P. Wuskell, L. M. Loew and S. D. Antic. "Intracellular long-wavelength voltage-sensitive dyes for studying the dynamics of action potentials in axons and thin dendrites," *J. Neurosci. Meth.* **164**(2): 225-239 (2007).

32. P. Yan et al., "Palette of fluorinated voltage-sensitive hemicyanine dyes," *Proc. Natl. Acad. Sci. USA* **109**(50), 20443-20448 (2012).

Figure Legend

Fig. 1 The imaging system. (a) Schematic of the imaging system including simultaneous UV/blue LED illumination and the dual-head CCD camera (illustrated in the picture) for simultaneous V_m and Ca^{2+} imaging; the image from the 60X objective is demagnified by a coupler before detection. (b) Images of a micrometer slide from the two aligned heads of the camera using 0.5X and 0.25X demagnifying couplers; the distance between two adjacent lines is 10 μm (c) Top: Fluorescence sub-images of the apical dendrite of a CA1 hippocampal pyramidal neuron filled with 1 mM OG5N; resting fluorescence from the V_m camera is <5% with respect to that from the Ca^{2+} camera; bottom: the fluorescence transient associated with an action potential is detected with the Ca^{2+} camera and it is negligible at the V_m camera. (d) Top: Fluorescence sub-images of the apical dendrite of another CA1 hippocampal pyramidal neuron filled with JPW1114; resting fluorescence from the Ca^{2+} camera is <5% with respect to that from the V_m CCD; bottom: the fluorescence transient associated with an action potential is detected with the V_m CCD and it is negligible at the Ca^{2+} camera.

Fig. 2 Calibration of JPW1114- $\Delta F/F_0$ in terms of ΔV_m . (a) Initial apical dendritic segment of a CA1 hippocampal pyramidal neuron loaded with the VSD JPW1114; the region from where fluorescence was averaged is outlined in yellow. (b) JPW1114- $\Delta F/F_0$ associated with an action potential or glutamate photorelease; the calibration protocol is applied from the resting membrane potential which is assumed to be uniform over the cell; the massive ionotropic glutamate receptors activation drives the illuminated dendritic area to 0 mV. The action potential trace is from an average of 32 trials; the calibration trace was from an average of 9 trials.

Fig. 3 Kinetics of different Ca^{2+} indicators investigated in voltage clamp. (a) Voltage clamp protocol consisting of two 16 ms voltage pulses from -70 mV, the first one below the threshold for activation of Ca^{2+} channels and the second one to ~ 20 mV; experiments were performed in the presence of Na^+ and K^+ channels blockers; the Ca^{2+} current (I_{Ca}) was extracted by subtraction of the scaled sub-threshold current; the kinetics of the current was analysed in correlation with that of the Ca^{2+} fluorescence change in the initial 60 μm segment of the apical dendrite; all data were averages of 16 trials. (b) I_{Ca} and $\text{Ca}^{2+} \Delta\text{F}/\text{F}_0$ from 5 representative cells filled with 1 mM of one of the following indicators OGB1, OG6F, OG5N, BF2 or FuraFF; the integrals of I_{Ca} ($\int I_{\text{Ca}}$) are also shown; signals are normalised to their maxima over the first 7 ms after the pulse beginning; simulations of the Dye- Ca^{2+} binding reaction are reported on the right. (c) From two the representative cells filled either with OGB1 or with OG5N the $\int I_{\text{Ca}}$ and $\text{Ca}^{2+} \Delta\text{F}/\text{F}_0$ normalised to their maxima over the first 4 ms after the pulse beginning; the difference between the two curves is also reported. (d) Mean \pm SD of the surface of $\int I_{\text{Ca}} - \Delta\text{F}/\text{F}_0$ (S) obtained for each of the 5 indicators tested from the number of cells reported; OGB1: 0.185 ± 0.034 , N=5; OG6F: 0.049 ± 0.023 , N=5; OGB1: 0.007 ± 0.018 , N=12; BF2: 0.375 ± 0.150 , N=4; FuraFF: 0.002 ± 0.023 , N=6; the values of S for OGB1 with respect to those for OG5N, and the values of S for BF2 with respect to those for FuraFF were significantly different (2P t-test, $p < 0.001^*$ and $p < 0.002^{**}$ respectively). Panels a and c were adapted from ¹⁰.

Fig. 4 Calibration of Ca^{2+} currents using Ca^{2+} photorelease. (a) OG5N- $\Delta\text{F}/\text{F}_0$ from the initial 80 μm segment of the cell shown on the top (region of fluorescence average outlined) associated with a depolarisation from -70 mV to -10 mV (top) and from -10 mV to +40 mV (bottom). (b) From the same cell filled with a solution containing 300 μM NP-EGTA and 150 μM CaCl_2 sequential UV-flashes (pulses) at -10 mV produced a OG5N- $\Delta\text{F}/\text{F}_0$ signal of decreasing amplitude (left); the OG5N- $\Delta\text{F}/\text{F}_0$ amplitude vs the pulse was fitted with a geometric sequence to obtain the efficiency of each pulse ($\alpha = 0.2$ in this example); considering the Ca^{2+} photoreleased by the first pulse a signal of 1% corresponded to $[\text{Ca}^{2+}]_{\text{TOT}} = 18 \mu\text{M}$ in this specific cell. (c) Calibrated OG5N- $\Delta\text{F}/\text{F}_0$ (middle trace) associated with an action potential (top trace) and corresponding I_{Ca}/V (bottom trace); Data are from an average of 64 trials. Panel a was adapted from ¹⁰.

Fig. 5 Extraction of the Ca^{2+} current using filtering or curve fitting. (a) Fluorescence images of a cell filled with OG5N; region A comprises $\sim 50 \mu\text{m}$ of dendrite from where fluorescence was averaged; region B is a single pixel. (b) Action potential signal from an average of 32 trials (left) or from a single trial (right). (c) From the same trials above, OG5N- $\Delta\text{F}/\text{F}_0$ signals from the average of 32 trials in region A (left), from the average of 32 trials in region B (middle) or from the single trial in region B (right); the signals were either unfiltered (top, blue traces), filtered with the Savitzky-Golay

algorithm at time windows of 10 (SG10), 20 (SG20) and 40 (SG40) samples, or fitted by the product of three sigmoid functions (FIT); the filter algorithm and the fit were implemented by the “smooth” and “lsqcurvefit” Matlab functions respectively. (d) From the filtered or the fitted traces above, the I_{Ca}/V were calculated for the three cases: average of 32 trials in region A (left), average of 32 trials in region B (middle) or single trial in region A (right); the approach of data fitting permits I_{Ca}/V extraction from sites of $\sim 2.4 \mu\text{m}$ using averaged trials or from larger regions in single trials.

Fig. 6 Dendritic I_{Ca}/V associated with an action potential at different starting V_m . (a) Fluorescence images of a cell filled with OG5N and JPW1114; the region from where fluorescence was average is outlined. (b) Optical measurements of V_m (top traces) and I_{Ca}/V (bottom traces) with an action potential starting either at $V_m = -60 \text{ mV}$ or -80 mV . (c) I_{Ca}/V superimposed to the optically recorded action potential in the two cases. (d) Mean \pm SEM of the peak I_{Ca}/V associated with an action potential starting either at $V_m = -60 \text{ mV}$ or $V_m = -80 \text{ mV}$ from 14 cells; the peak I_{Ca}/V was significantly higher for the action potential starting at -80 mV ($p < 0.001$, paired t-test).

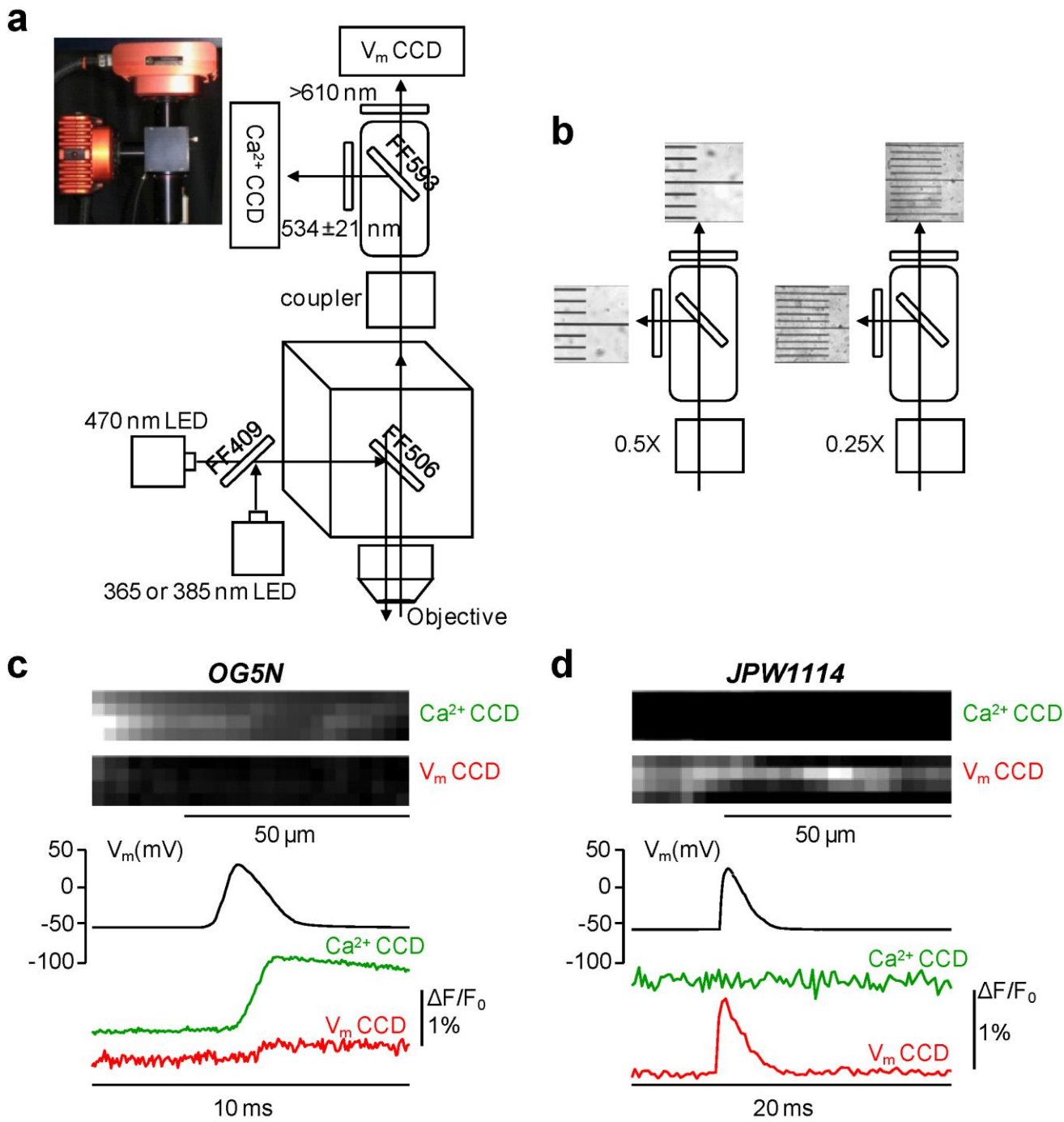


Fig1

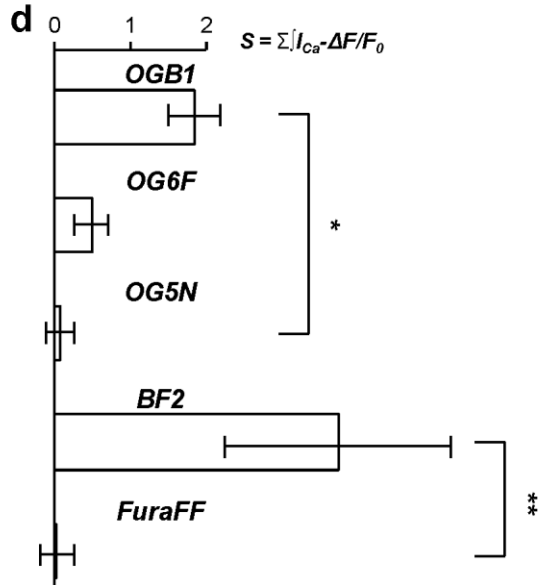
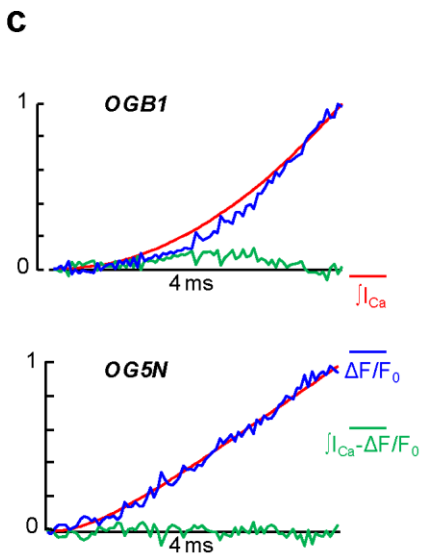
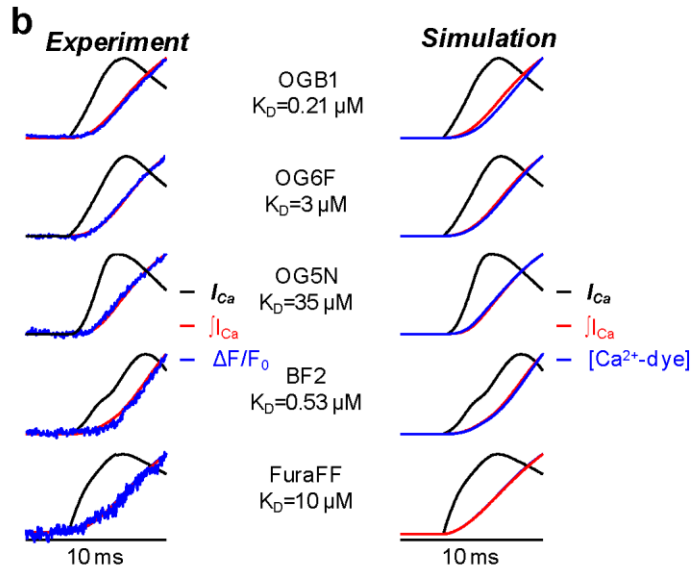
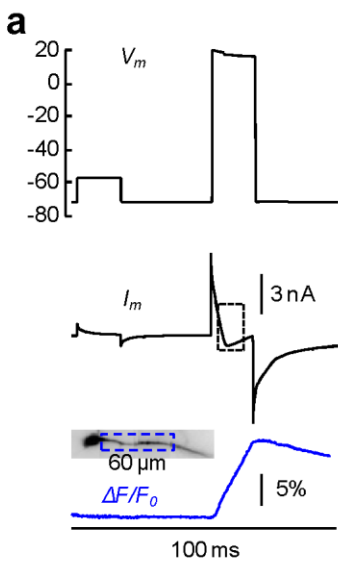
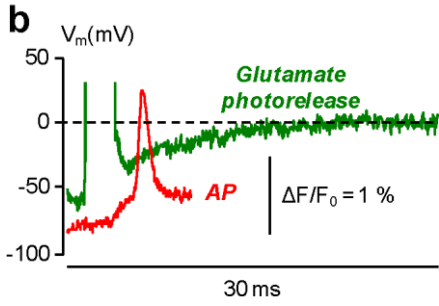
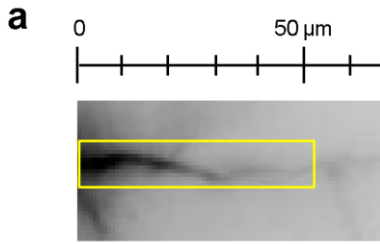


Fig3

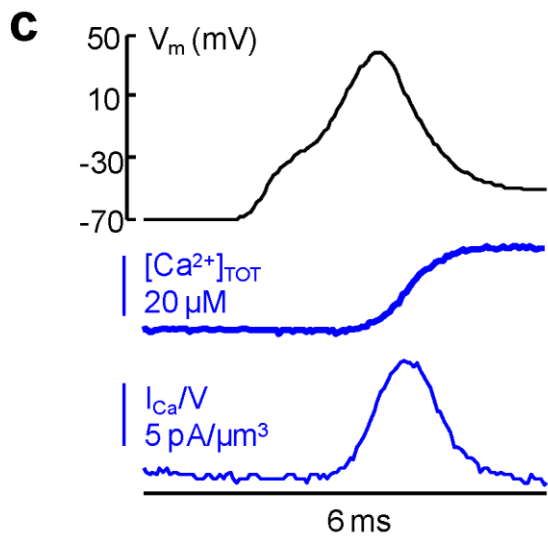
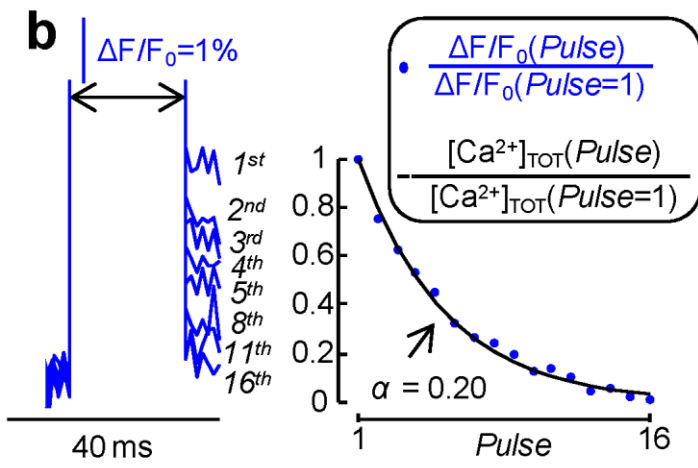
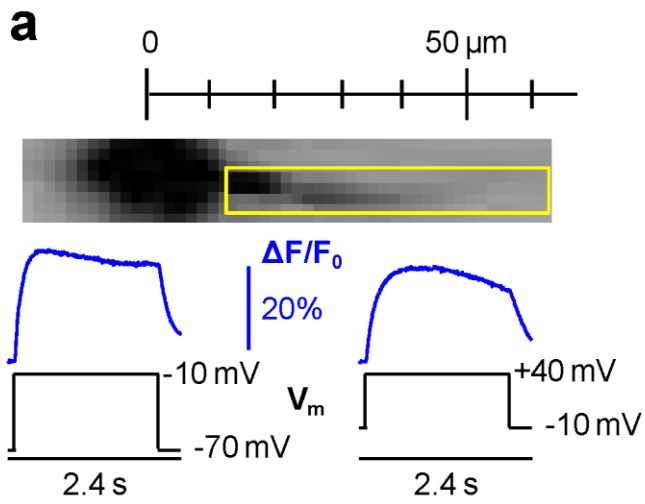


Fig4

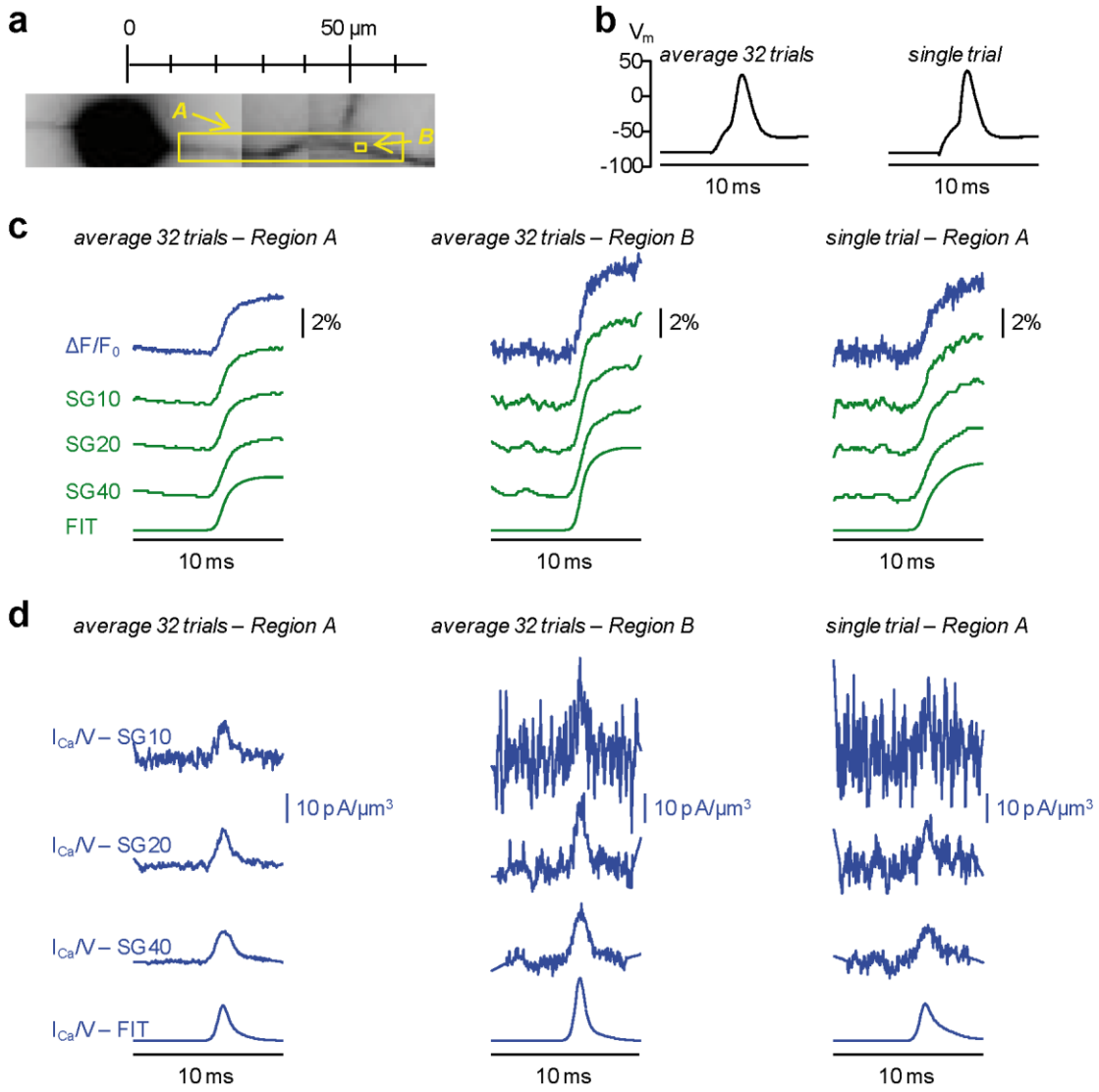


Fig5

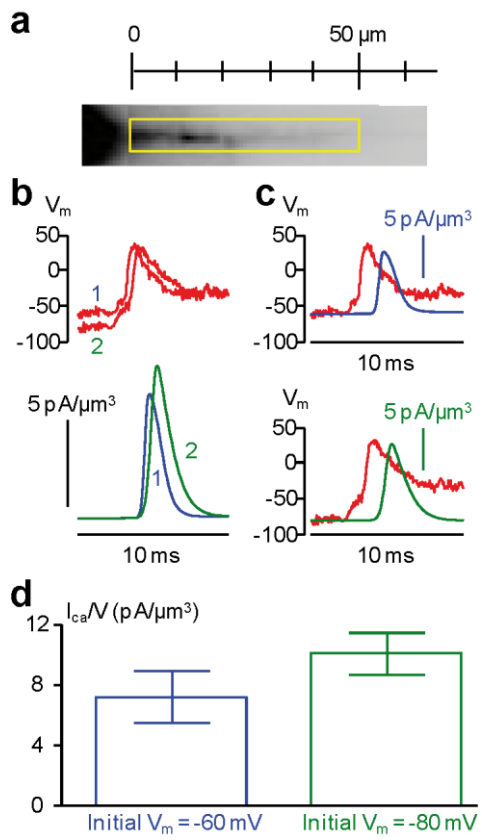


Fig6